Physics of the Solid State, 2025, Vol. 67, No. 3

04,09

Formation of electroinduced near-surface layers in the polar direction of triglycine sulfate crystals

© *V.I. Akkuratov, A.G. Kulikov¶, Yu.V. Pisarevsky, E.S. Ivanova*

A.V. Shubnikov Institute of Crystallography of the Kurchatov Complex for Crystallography and Photonics
of National Research Center „Kurchatov Institute,“
Moscow, Russia

¶ E-mail: ontonic@gmail.com

Received January 22 2025
Revised March 11, 2025
Accepted March 12, 2025

Using the X-ray topography method, images of near-surface charge layers in pyroelectric crystal of triglycine sulfate were obtained for the first time. These charge layers were formed by internal field of triglycine sulfate crystal and by applied external electric field along the polar direction [010]. These layers were detected by increase in the integral intensity of X-ray radiation, which indicates the formation of an extinction contrast for the diffraction reflection 060 and much less pronounced changes for 400 reflection. With an increase in the external field strength up to 150 V/mm, an increase in the intensity in these regions and no changes in the center of the crystal were observed, which indicates compensation of the electric field in the volume due to the accumulation of charge carriers in a layer with a thickness of 1 mm. This effect depends on the polarity and is reversible when the external electric field is removed. Application of the field along the non-polar direction [100] does not lead to changes in the topograms.

Keywords: near-surface charged layer, X-ray diffractometry, X-ray topography, ferroelectrics, external electric field, charge carrier migration.

DOI: 10.61011/PSS.2025.03.60874.16-25

1. Introduction

It is well known that polar crystals have space charge regions (SCR) induced by spontaneous polarization near the surface [1] that compensate the electric field within a crystal. Despite large-scale application of pyroelectrics, the structure of these compensating charged layers was almost undiscovered. At the same time, it is important to study the structure and formation dynamics of near-surface charge carrier layers both in terms of fundamental research and due to the focus on practical application in compact and energy-saving devices [2].

In dielectric crystals with a band gap of several eV, the main contribution to conductivity at room temperature is made by ion-vacancy type charged defects. Non-contact X-ray diffraction test methods are an effective and sensitive tool for examination of defects [3], electromechanical [4], magnetostriction [5] and piezoelectric [6] deformations. In particular, X-ray diffraction methods were used in [7,8] to record formation of near-surface oxygen vacancy layers with a thickness in the order of μm in paratellurite and strontium titanate crystals in a strong (~ 1000 V/mm) external electric field. These crystals are classified as nonpolar, and a double electric layer is not formed in them when an external field is not available.

Triglycine sulfate (TGS) crystal is a polar dielectric. An important advantage of the TGS crystal for X-ray diffraction experiments is its composition consisting of light atoms that allows „transmission“ diffraction examination for data recording from the whole volume of the sample [9]. X-ray topography method allows high spatial resolution display of lattice distortions using contrast formed by the interference of beams diverging from the defect [10,11].

This study included X-ray topographic survey of the formed near-surface charged layers consisting of point defects in ferroelectric TGS crystals without and with constant external electric field.

2. Samples and research methods

2.1. Samples

Perfect TGS single crystals are widely used as detector elements for IR spectroscopy due to remarkable pyroelectric properties [12,13]. TGS has monoclinic space group $P2_1$. Lattice cell parameters at room temperature: $a = 9.419$ Å, $b = 12.647$ Å and $c = 5.727$ Å with angles $\alpha = \gamma = 90°$, $\beta = 110.4°$ [14,15]. TGS has cleavage in the $\langle 010 \rangle$ planes [16]. Polar axis coincides with the b axis. Boundaries of ferroelectric 180-degree domains in TGS coincide with the boundaries of twins [17] and elongated along the [010] polar axis. Voltage needed for domain switching is determined by coercive and saturating electric fields [18]. Piezoelectric coefficients acting along the polar direction are as follows $d_{21} = 28$ pC/N, $d_{22} = 45$ pC/N, $d_{23} = -85$ pC/N and $d_{25} = -10$ pC/N [19]. The crystal band gap is more than 5 eV. Permittivity ε_{22} in TGS at room temperature is 43. Spontaneous polarization falls to 0 during heating to the phase transition at 49 °C [20]. Temperature dependence of

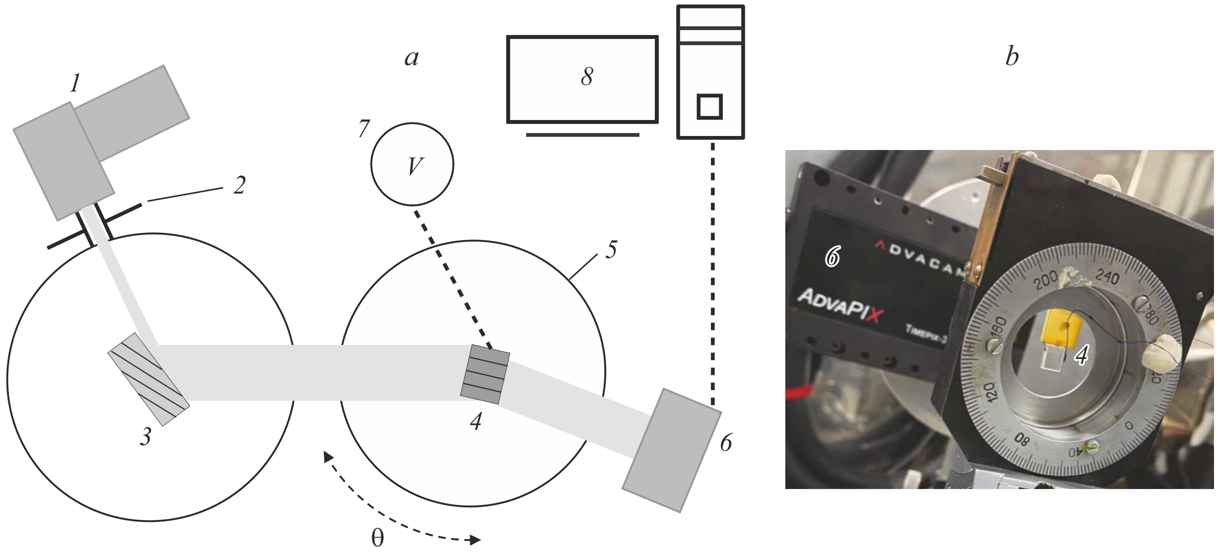

Figure 1. (*a*) X-ray optic scheme for double-crystal topography experiments contains an X-ray source (*1*), diaphragm (*2*), asymmetric crystal monochromator (*3*), test sample (*4*), goniometric system (*5*), two-dimensional detector *6*, external electric field supply system on the basis of a high-voltage source (*7*), control computer (*8*). (*b*) Photo of a crystal holder with a fixed TGS sample and a detector placed behind the sample.

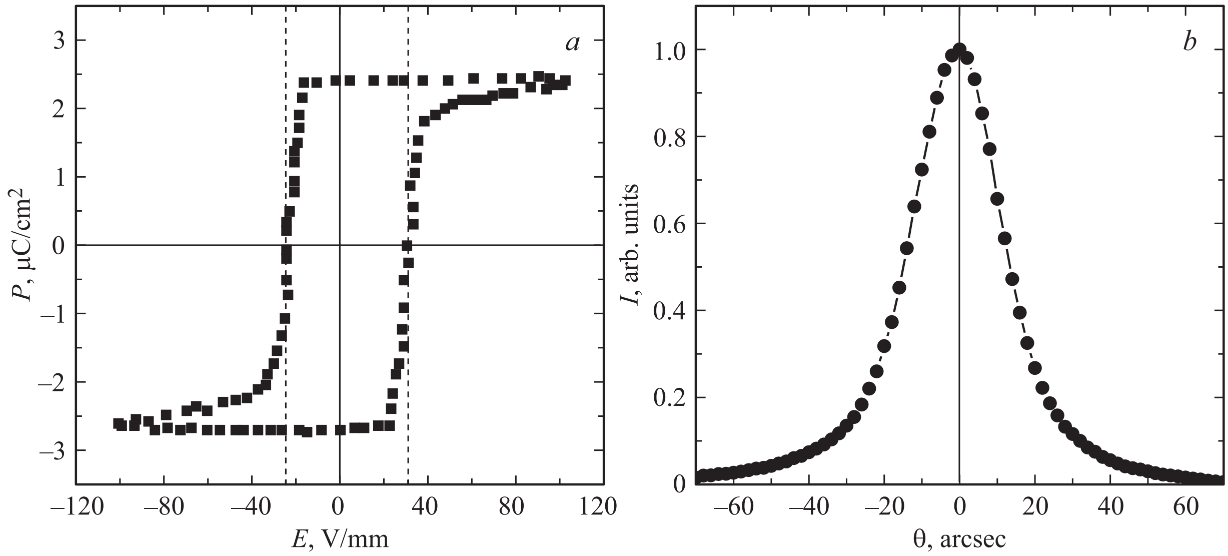

Figure 2. (*a*) Dielectric hysteresis loop $P(E)$ of the studied TGS crystal. (*b*) Initial RC, reflection 060, obtained from the whole crystal volume in the „transmission" diffraction configuration without an external electric field.

dielectric properties and spontaneous polarization near the Curie point was studied in [21,22].

Electric conductivity of TGS in weak (in the order of some V/mm) fields was studied in [23]. Relaxation behavior of conductivity, high dependence on bias voltage and temperature are indicative of the polaron charge transfer mechanism [24]. Conductivity along *b* is primarily implemented by means of hops between glycine ions. In this case, a space charge is formed to limit the flowing current.

High quality TGS seed single crystals grown by Fundamental Scientific Research Center „Crystallography and Photonics" RAS (now Kurchatov Complex for Crystallography and Photonics of NRC „Kurchatov Institute") were used as samples for the X-ray diffraction experiments. The TGS samples were cut in the form of 7×8 mm rectangular crystal plates with side faces perpendicular to the [100] and [010] crystallographic directions, respectively, that are orthogonal between each other. When preparing the test samples, cleavage property was used to achieve ideally smooth clean surfaces at crystal faces. Sample thickness was 3 mm. Conductive silver electrodes were applied to the crystal faces corresponding to the $\langle 010 \rangle$ planes to generate a uniform electric field along the polar direction within the crystal. Thin copper wires were soldered to the electrodes

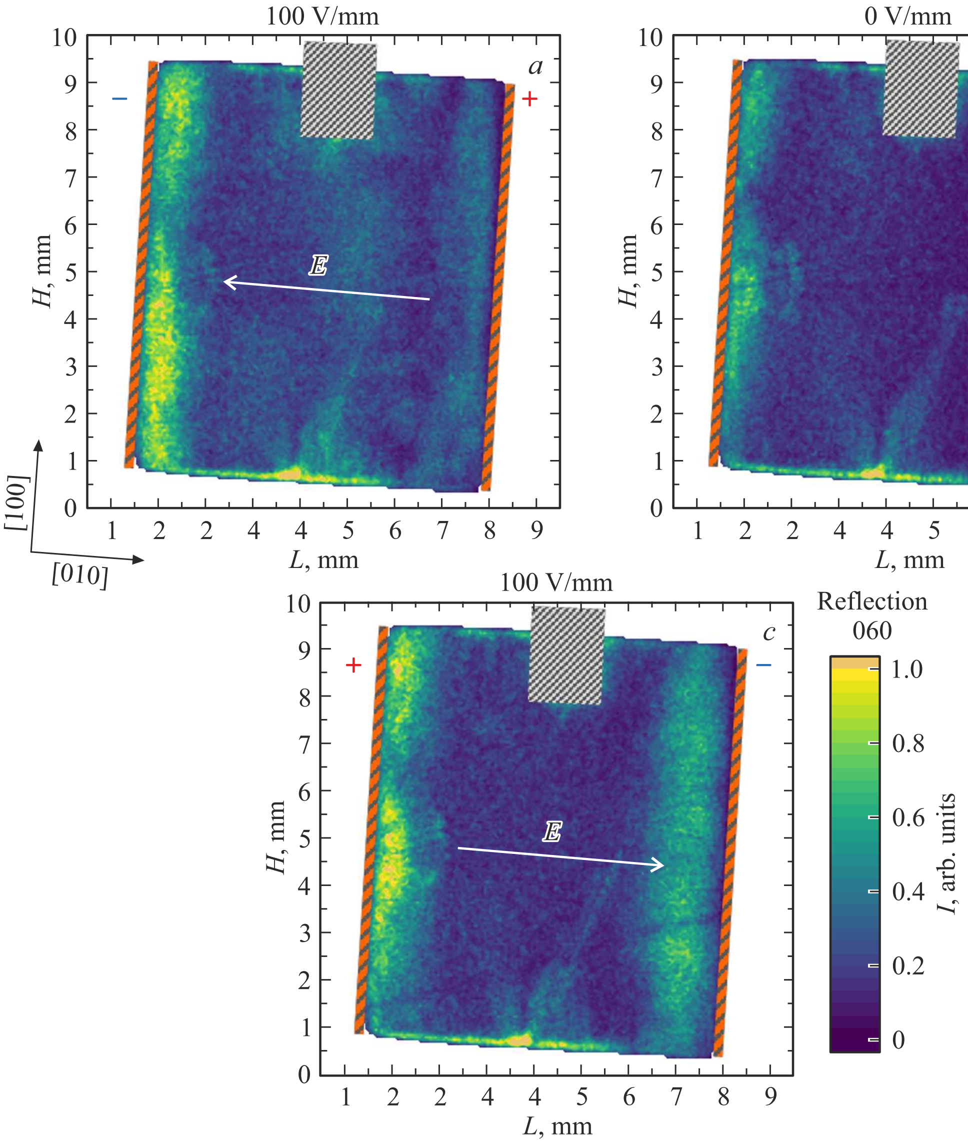

Figure 3. Spatial integral intensity distribution of diffraction reflection 060 of the TGS crystal without an applied electric field (*b*) and in an external electric field of both polarities (*a, c*). Electric field *E* with a strength of 100 V/mm is applied along the [010] polar axis. Sign corresponds to the external potential on the electrode. Crystal attachment zone is grey, electrodes are orange.

and connected to a high-voltage source. The crystal was fixed in an electrically insulated crystal holder.

2.2. Procedure and equipment

The main experiments used a double-crystal X-ray topography method implemented on a triple-axis X-ray spectrometer (TXS). The experiment setup is shown in Figure 1. X-ray Mo tube with $\lambda[\mathrm{Mo}K_{\alpha 1}] = 0.70932\,\text{Å}$ was used as a radiation source. A Si (440) monochromator with a asymmetry factor of 0.025 and a 150 μm slit installed in front of it allows X-ray beam broadening to a cross-section in the order of cm with spatial separation of the doublet K_α. The sample was aligned in the holder using a set of linear and angular adjusters on a multi-circle goniometer with scanning capability along the θ and 2θ axes with an accuracy of 0.1 arcsec. Topographic images were made using the Advacam TimePix TPX3 two-dimensional CdTe detector with 256 × 256 pixels and the pixel size of 55 μm.

The sample was set to a diffraction position corresponding to reflections with Miller indices 060 and 400 with the Bragg angles $\theta_{400} = 18.495^\circ$ and $\theta_{060} = 19.378^\circ$, respectively. Diffraction reflection parameters of the crystal were evaluated using X-ray Server online program [25]. Calculated Darwin rocking curve (RC) has FWHM of 0.33 arcsec with the extinction depth $L_{\mathrm{ext}} = 263\,\mu$m for reflection 060 and of 0.25 arcsec with $L_{\mathrm{ext}} = 357\,\mu$m. Linear absorption coefficient for TGS is 2.5 cm^{-1}.

X-ray topographic images were made in the integral intensity accumulation mode that implies diffraction pattern recording by a two-dimensional detector in course of angular scanning with set exposure time and pitch on the axis θ

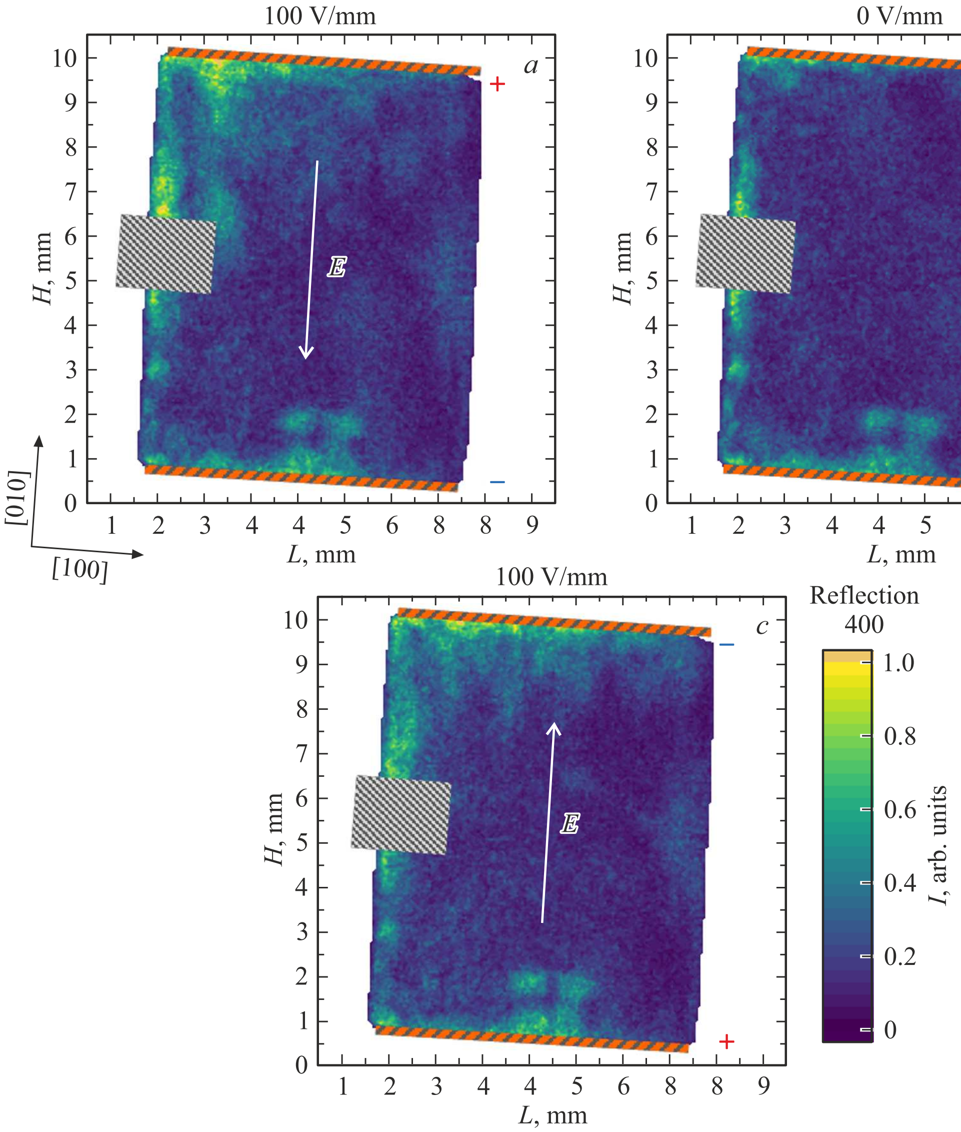

Figure 4. Spatial integral intensity distribution of diffraction reflection 400 of the TGS crystal without an applied electric field (b) and in an external electric field of both polarities (a, c). Electric field E with a strength of 100 V/mm is applied along the [010] polar axis. Sign corresponds to the external potential on the electrode. Crystal attachment zone is grey, electrodes are orange.

near the diffraction reflection maximum. Scanning range was 140 arcsec, scanning pitch was 2 arcsec, point exposure time was 1 s, total topogram measurement time was about 90 s. Electric field was applied to the sample using the Keithley 2290-5 high-voltage source. The transmission configuration was used to record topograms formed from the whole crystal volume.

Information regarding ferroelectric properties and structural perfection of the prepared sample was obtained using the Sawyer-Tower method for measuring dielectric hysteresis loops $P(E)$.

3. Experimental results and discussion

Before the X-ray experiment, dielectric hysteresis loops $P(E)$ were measured in a quasistatic mode at 7 Hz on the prepared sample. They had an almost symmetric form, and coercive field values EC were -25 and $+29$ V/mm (Figure 2, a). Such coercive field values confirm high quality of the TGS crystal used for the experiments.

Double-crystal RC of the TGS crystal, reflection 060, had a symmetric Gaussian form with FWHM of 28.3 arcsec (Figure 2, b). Taking into account the aspects of water-soluble crystal growth and inadvertent presence of defects such as dislocations and inclusions in the crystals [26,27], the plotted RCs are indicative of high perfection of the real crystal structure.

Then, topograms of the TGS sample were made before the application of an external electric field and during application of a field with a preset strength along the [010] polar direction. Two identical measurement series were carried out for reflections 060 and 400, respectively (Figures 3

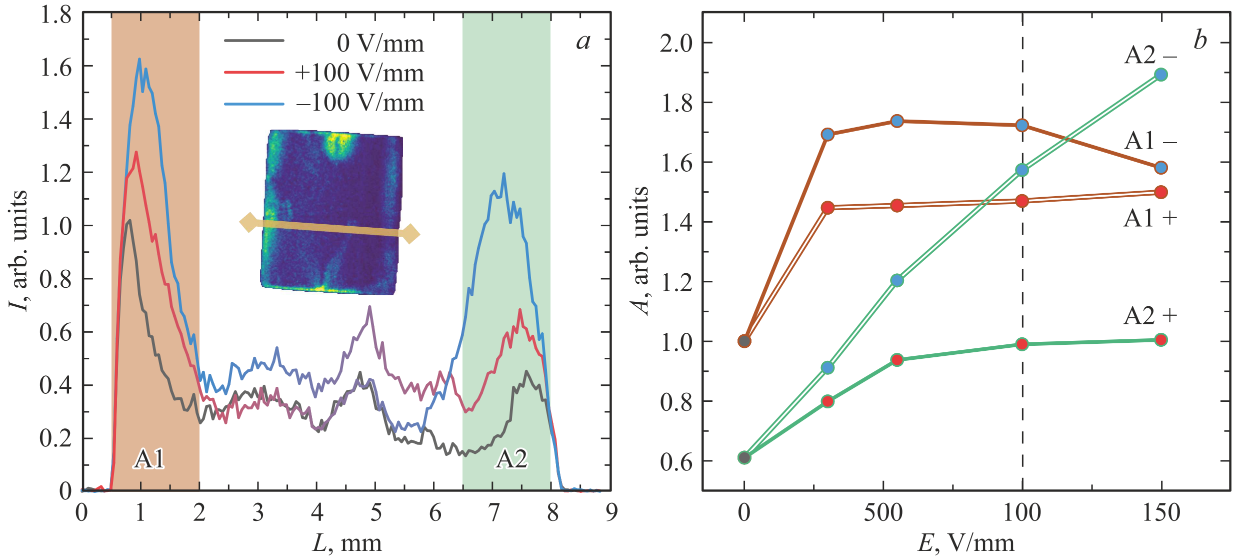

Figure 5. (a) Integral intensity distribution profiles for reflection 060 depending on the coordinate along the [010] crystallographic direction of TGS when the 100 V/mm external electric field with different polarity is applied along the [010] crystallographic direction. The profile plotting line is shown schematically in the inserted topogram. Values on the diagrams are reduced to the maximum value for curve $E = 0$ V/mm. Red (+) and blue (−) colors on the diagrams correspond to the potential on the nearest electrode. Brown and green regions A1, A2 correspond to the summation regions 1.5 mm in width. (b) Dependence of the integral intensity growth of diffraction reflection 060 in regions A1, A2 and two electrode potential signs (+, −) on the applied external voltage. Dashed line corresponds to the 100 V/mm field.

and 4). External electric field of both polarities with strength $E = 30$, 55, 100 and 150 V/mm was applied to the crystal.

When a field was applied for reflection 060, areas with increased integral intensity were formed near the electrodes compared with the initial state and mean integral intensity in the crystal volume (Figure 3). The opposite-polarity field changes the intensity distribution pattern. The greatest growth of intensity is observed near the negative potential electrode. For reflection 400, integral intensity variation near the electrodes is much weaker (Figure 4).

Intensity growth is generally indicative of deformations in a particular crystal region. Deformation gradient leads to intensity redistribution between direct and diffracted radiation and to extinction contrast on the topogram [28]. Deformation accumulation may appear during migration of charged defects [29] and defect clusters [30].

Figure 5, a shows topogram cross-sections of reflection 060, i. e. curves of integral intensity distribution along the electric field application direction [010] for the field strength of 100 V/mm. Space intensity integration regions near the electrodes are highlighted in color, the integration results were used to plot the dependence in Figure 5, b for both electric potential signs on the corresponding electrodes. It is clearly seen that the integral intensity grows mainly near the electrodes, which corresponds to charge carrier accumulation in the layer with an effective thickness in the order of 1 mm. Thus, a charge carrier concentration and screening field gradient is formed in depth along the polar direction.

Screening field and its distributions in the near-electrode region appear through the inverse piezoelectric effect. In the configuration of our experiment, possible variations of the monoclinic angle β between [100] and [001] are insensitive to reflection 060. Intensity variation of reflection 060 is possible only by means of activation the tension/compression piezoelectric constants d_{22} and d_{23} with inhomogeneous distribution of charge carriers near the electrodes, which will provide bending of reflecting planes. Thus, the deformation gradient in the near-electrode region formed by the screening fields and oriented along scattering vector 060 give rise to a significant extinction contrast.

For measurement of reflection 400, the scattering vector is perpendicular to the field direction and, accordingly, to the gradient of deformation arising along [010]. A slight moire in Figure 4, a and 4, c occurs due to a possible inhomogeneous configuration of a compensating layer along the electrode.

In case of polarity inversion (Figure 3), the intensity distribution is not fully inverted. This fact may be due to the residual polarization effect in the TGS crystal resulting from the existence of an immobile SCR of charged defects at the boundaries, which is demonstrated by a brighter region in the topogram near one of the electrodes with $E = 0$ V/mm (Figure 3, b). Thus, the presence of residual ion-vacancy type SCRs is the factor due to which a difference may occur in charge carrier layer configuration on different sides of the crystal (Figure 5).

Reversibility of the effect is confirmed by the fact that all accumulated deformations disappear immediately when the field is switched off, and the intensity distribution in the topogram returns to its initial state.

It is important that a field applied along [100] perpendicular to the polar direction doesn't induce deformation regions near the electrodes at the corresponding edges, which is displayed as the absence of intensity variation in the topograms both for reflection 400 and 060.

4. Conclusion

The double-crystal X-ray topography method first detected the formation of space charge regions near the TGS crystal electrodes. The effect is demonstrated as the increase in integral intensity of diffraction reflection 060 due to the extinction contrast on the deformations caused by charge carrier clusters. These near-surface charged layers are formed due to the spontaneous polarization and in the external electric field applied along the [010] polar direction. Topograms demonstrate that charge carriers are grouped in a comparatively long region with a thickness up to 1 mm to compensate the internal crystal field. Charge carriers are grouped at a distance in the order of half layer thickness, rather than directly against the electrodes.

Dependence of deformation distribution on the external electric field polarity, anisotropy of defect formation along the [100] and [010] crystallographic directions, and nonlinear defect behavior vs. external field strength with attainment of saturation are among the key features of the effect observed in TGS. It is important that the integral intensity pattern returns to its initial state when the electric field is removed, regardless of the fact that the applied field exceeds the coercive field considerably.

The obtained results, on the one hand, demonstrate the capabilities of the extensively developed class of *in-situ* X-ray diffraction methods implemented, in particular, in synchrotron sources, and, on the other hand, may serve as the basis for obtaining important details concerning the impact of a defect structure on the formation of electric fields in pyroelectrics, which can be used for currently developed electronic and storage systems.

Acknowledgments

The authors are grateful to E.D.Yakushkin (National Research Center „Kurchatov Institute“) for their assistance in dielectric hysteresis loop measurements.

Funding

This study was carried out under the state assignment of NRC „Kurchatov Institute“.

Conflict of interest

The authors declare no conflict of interest.

References

[1] W. Känzig. Phys. Rev. **98**, *2*, 549 (1955). DOI: https://doi.org/10.1103/PhysRev.98.549

[2] B.B. Tian, Y.Liu, L.F. Chen, J.L.Wang, S. Sun, H. Shen, J.L. Sun, G.L. Yuan, S. Fusil, V. Garcia, B. Dkhil, X.J. Meng, J.H. Chu. Sci. Rep., **5**, *1*, 18297 (2015). DOI: https://doi.org/10.1038/srep18297.

[3] D.A. Zolotov, A.V. Buzmakov, D.A. Elfimov, V.E. Asadchikov, F.N. Chukhovskii. Crystallogr. Rep. **62**, *1*, 20 (2017).

[4] A.G. Kulikov, N.V. Marchenkov, A.E. Blagov, K.G. Kozhemyakin, M.Yu. Nasonov, S.S. Pashkov, Yu.V. Pisarevskii, G.N. Cherpukhina. Acoust. Phys. **62**, *6*, 694 (2016). DOI: 10.1134/S1063771016050080

[5] N.I. Snegirev, A.G. Kulikov, I.S. Lyubutin, A.Yu. Seregin, S.V. Yagupov, M.B. Strugatsky. JETP Letters **119**, *6*, 464 (2024). DOI: 10.1134/S0021364024600484

[6] E.S. Ibragimov, A.G. Kulikov, N.V. Marchenkov, Yu.V. Pisarevsky, A.E. Blagov, M.V. Kovalchuk. Phys. Solid State **64**, *11*, 1723 (2022). DOI: 10.21883/PSS.2022.11.54197.421

[7] A.G. Kulikov, A.E. Blagov, N.V. Marchenkov, V.A. Lomonov, A.V. Vinogradov, Yu.V. Pisarevsky, M.V. Kovalchuk. JETP Letters **107**, *10*, 646 (2018). DOI: 10.1134/S0021364018100120

[8] J. Hanzig, M. Zschornak, F. Hanzig, E. Mehner, H. Stöcker, B. Abendroth, C. Röder, A. Talkenberger, G. Schreiber, D. Rafaja, S. Gemming, D.C. Meyer. Phys. Rev. B. **88**, 024104 (2013). DOI: https://doi.org/10.1103/PhysRevB.88.024104

[9] V. Akkuratov, A. Kulikov, Yu. Pisarevsky, A. Blagov, M. Kovalchuk. J. Appl. Crystallogr. **56**, *1*, (2023). DOI: 10.1107/S1600576722012183

[10] V.V. Lider. Phys. Solid State **63**, 189 (2021). DOI: 10.21883/FTT.2021.02.50461.212

[11] D. Bowen, B. Tanner. High resolution X-ray diffractometry and topography. CRC press. (1998) 252 p.

[12] C. Bowen, J. Taylor, E. Leboulbar, D. Zabek, A. Chauhan, R. Vaish. Energy Environ. Scie. **7**, 10 (2014). DOI: https://doi.org/10.1039/C4EE01759E

[13] R.W. Whatmore. Rep., Prog. Phys. **49**, 12 (1986). DOI: 10.1088/0034-4885/49/12/002

[14] S. Fletcher, E. Keve, A. Skapski. Ferroelectrics **14**, 775 (1976). DOI: https://doi.org/10.1080/00150197608237797

[15] M. Kay, R. Kleinberg. Ferroelectrics **5**, 45 (1973). DOI: https://doi.org/10.1080/00150197308235778

[16] N. Nakatani. Jpn. J. Appl. Phys. **18**, *3*, 491 (1979). DOI:

[17] V.P. Konstantinova, I.M. Sil'vestrova, V.A. Yurin, Kristallografiya **4**, 125 (1959). DOI: 10.1143/JJAP.18.491

[18] R. Gainutdinov, E. Ivanova, E. Petrzhik, A. Lashkova, T. Volk. JETP Letters **106**, 97 (2017). DOI: https://doi.org/10.1134/S0021364017140053

[19] V.P. Konstantinova, I.M. Silvestrova, K.S. Aleksandrov. Sov. Phys. Crystallogr. **4**, *1*, 69 (1959).

[20] C.J. Raj, S. Kundu, K.B.R. Varma. Appl. Phys. A **105**, 1025 (2011). DOI: https://doi.org/10.1007/s00339-011-6541-7

[21] S. Hoshino, T. Mitsui, F. Jona, R. Pepinsky. Phys. Rev. **107**, *5*, 1255 (1957). DOI: https://doi.org/10.1103/PhysRev.107.1255

[22] S. Triebwasser. IBM J. Res. Dev. **2**, *3*, 212 (1958). DOI: 10.1147/rd.23.0212

[23] W. Osak, K. Tkacz-Smiech, C. Strzalkowska. Ferroelectrics **158**, *1*, 331 (1994). DOI: https://doi.org/10.1080/00150199408216038

[24] W. Osak. Z. Naturforsch. A **52**, 621 (1997). DOI: https://doi.org/10.1515/zna-1997-8-913

[25] „X-ray Server“ online program website https://x-server.gmca.aps.anl.gov/x0h.html

[26] R.B. Lal, A.K. Batra. Ferroelectrics **142**, 51 (1993). DOI: 10.1080/00150199308237884

[27] A. Izrael, J.F. Petroff, A. Authier, Z. Malek. J. Cryst. Growth **16**, *2*, 131 (1972). DOI: 10.1016/0022-0248(72)90104-2

[28] A. Authier. Adv. X-ray Anal. **10**, 9 (1966).

[29] J. Hanzig, M. Zschornak, E. Mehner, F. Hanzig, W. Münchgesang, T. Leisegang, H. Stöcker, D.C. Meyer. J. Phys. Condens. Matter **28**, 225001 (2016). DOI: 10.1088/0953-8984/28/22/225001

[30] C. Ludt, E. Ovchinnikova, A. Kulikov, D. Novikov, S. Gemming, D.C. Meyer, M. Zschornak. Crystals **11**, 693 (2021). DOI: 10.3390/cryst11060693

Translated by E.Ilinskaya